

## Analysis of secondary electron emission for conducting materials using 4-grid LEED/AES optics

This content has been downloaded from IOPscience. Please scroll down to see the full text.

2015 J. Phys. D: Appl. Phys. 48 195204

(<http://iopscience.iop.org/0022-3727/48/19/195204>)

View [the table of contents for this issue](#), or go to the [journal homepage](#) for more

Download details:

IP Address: 198.35.0.177

This content was downloaded on 16/04/2015 at 17:41

Please note that [terms and conditions apply](#).

# Analysis of secondary electron emission for conducting materials using 4-grid LEED/AES optics

M I Patino<sup>1</sup>, Y Raitsev<sup>2</sup>, B E Koel<sup>3</sup> and R E Wirz<sup>1</sup>

<sup>1</sup> Department of Mechanical and Aerospace Engineering, University of California, Los Angeles, CA 90095, USA

<sup>2</sup> Princeton Plasma Physics Laboratory, Princeton, NJ 08543, USA

<sup>3</sup> Department of Chemical and Biological Engineering, Princeton University, Princeton, NJ 08540, USA

E-mail: [mipatino@ucla.edu](mailto:mipatino@ucla.edu)

Received 27 October 2014, revised 24 February 2015

Accepted for publication 2 March 2015

Published 8 April 2015



CrossMark

## Abstract

A facility utilizing 4-grid optics for LEED/AES (low energy electron diffraction/Auger electron spectroscopy) was developed to measure the total secondary electron yield and secondary electron energy distribution function for conducting materials. The facility and experimental procedure were validated with measurements of 50–500 eV primary electrons impacting graphite. The total yield was calculated from measurements of the secondary electron current (i) from the sample and (ii) from the collection assembly, by biasing each surface. Secondary electron yield results from both methods agreed well with each other and were within the spread of previous results for the total yield from graphite. Additionally, measurements of the energy distribution function of secondary electrons from graphite are provided for a wider range of incident electron energies. These results can be used in modeling plasma-wall interactions in plasmas bounded by graphite walls, such as are found in plasma thrusters, and divertors and limiters of magnetic fusion devices.

Keywords: secondary electron emission, particle-material interaction, energy distribution function

(Some figures may appear in colour only in the online journal)

## Nomenclature

$\Theta$	grid half-angle	$E_{PE}^{\max}$	primary electron beam energy at maximum total secondary electron yield
$\Phi_{G1}$	G1 grid work function	$E_{SE}$	secondary electron energy with respect to the sample vacuum level
$\Phi_{G2,3}$	G2 and G3 grids work function	f	fraction of true secondary electrons with energy below the sample electrostatic potential
$\Phi_{G4}$	G4 grid work function	g	fraction of secondary electrons collected on each grid for unobstructed grid with zero grid transparency
$\Phi_{HS}$	hemispherical screenwork function	$I_{BE}$	backscattered electron current
$\Phi_S$	sample work function	$I_C$	collector current
$\alpha$	variance of Gaussian fit to total secondary electron yield	$I_{HS}$	hemispherical screen current
$\delta$	yield of true secondary electrons	$I_{PE}$	primary electron beam current
$\eta$	yield of backscattered electrons	$I_{RE}$	rediffused electron current
$\lambda$	mean free path	$I_S$	sample current
$\sigma$	total secondary electron yield, collision cross section	$I_{SEE}$	total secondary electron current
$\sigma_{\max}$	maximum total secondary electron yield	$I_{TE}$	true secondary electron current
$E_{PE}$	primary electron beam energy		

k	Boltzmann constant
L	distance from sample to LEED/AES optics
N	number of grids in front, number of secondary electrons with energy $E_{SE}$
n	number density
t	grid transparency
$V_{G1}$	G1 grid electrostatic potential
$V_{G2,3}$	G2 and G3 grids electrostatic potential
$V_S$	sample electrostatic potential
$V_{HS}$	hemispherical screen electrostatic potential

## 1. Introduction

Electron bombardment of materials leads to the emission of electrons from the materials (termed total secondary electrons) that may have a significant impact on the sheath and overall plasma behavior. In a plasma system (e.g. electric propulsion devices, divertors and limiters of magnetic fusion devices, and plasma processing systems), electrons with sufficient energy to overcome the wall sheath potential can impact the wall and produce secondary electrons. This secondary electron emission (SEE) can then reduce the potential at the wall, leading to an increased loss of plasma electrons to the wall, increased wall heating, and increased cooling of the bulk plasma [1, 2]. In particle accelerators (e.g. with positron beams), particle impact and cyclotron radiation incident on the walls can produce electrons that themselves can interact with the wall and lead to SEE. This multipacting effect [3] can create a cloud of electrons that may lead to instabilities in the particle beams and overheating of facility components [4]. For the aforementioned applications it is important to know the number and types of secondary electrons produced as well as the energies at which they are emitted from the surface. Note that ions can also produce electron emission from materials. However, in systems with ion beams and plasmas, ion-initiated electron emission is approximately one to two orders of magnitudes lower than the SEE in systems with electron beams and plasmas (where yields are near or greater than unity). While ion-initiated electron emission is important for devices such as cathodes (where it is required to sustain the plasma discharge) and electron multipliers for detectors in mass spectrometry, the focus herein will be on SEE initiated by primary electrons.

Secondary electrons are classified based on how they are produced: backscattered electrons, rediffused electrons, and true secondary electrons [5–9]. Backscattered electrons are incident primary electrons that are elastically reflected by atoms at the surface of the material and hence are at the energy of the primary electron  $E_{PE}$ . Rediffused electrons with energies between 50 eV and  $E_{PE}$  are primary electrons that have undergone inelastic collisions and have lost energy due to collisions with core and continuous-band electrons and from phonon and plasmon generation [6–9]. Note that Auger electrons, although a product of the Auger process, are often grouped with rediffused electrons [8]. True secondary electrons are electrons originally from within the material that are ejected after ionization or excitation of atoms by primary

electron impact and overcome the material work function; these true secondary electrons, by convention, are at energies below 50 eV [8].

Previous investigations into SEE from conducting materials has led to many empirical equations for the dependence of the total SEE yield  $\sigma$  (i.e. ratio of the number of electrons emitted from the material to the number of incident electrons) with incident energy [4, 8, 10–16] and angle [10, 11] with respect to the surface, as well as semi-empirical equations for the energy, angular, and spatial distribution [10] of the emitted secondary electrons. Measurements were made by exposing a sample of the material to a monoenergetic electron beam of known current  $I_{PE}$  and measuring (i) the sample current  $I_S$  [17, 18] or (ii) the current on a collecting electrode surrounding the sample  $I_C$  [16, 19]. The total yield  $\sigma$  is then

$$\sigma = \frac{I_{SEE}}{I_{PE}} = \frac{I_{PE} - (I_{PE} - I_{SEE})}{I_{PE}} = \frac{I_{PE} - I_S}{I_{PE}} = 1 - \frac{I_S}{I_{PE}} \quad (1)$$

$$\sigma = \frac{I_{SEE}}{I_{PE}} = \frac{I_C}{I_{PE}}. \quad (2)$$

In addition, the contributions from the backscattered, rediffused, and true secondary electrons were measured by inserting a hemispherical electrode in front of a hemispherical collector and applying a retarding potential to the electrode to separate out the true secondary electrons [12, 13, 20, 21].

This paper outlines the use of a common commercial surface analysis instrument to characterize SEE properties of conducting materials. A device utilizing 4-grid optics for LEED/AES (low energy electron diffraction/Auger electron spectroscopy), which has an integral electron gun, was used to measure the total SEE yield and energy distribution function of secondary electrons from graphite for primary electrons between 50 and 500 eV. Conventionally this instrument is used in surface science studies for LEED to determine the surface structure and long-range order of materials (from the position and intensity of the diffracted spots of the elastically scattered electrons on the hemispherical phosphor screen typically using 50–100 eV primary electrons incident on the material) and for AES to determine the surface elemental composition of the material (from the measured energy and number of the Auger electrons produced from bombardment of the material typically by high energy, i.e. 2–5 keV, primary electrons and by using the 4-grid optics as a retarding field analyzer). The primary electron current was measured by applying an increasingly positive bias on the sample and taking the sample current at 50 V. As was done by Pedgley *et al* [12] in conjunction with Farhang *et al* [13], and by Cimino and Collins [22], the SEE yield was calculated using two methods for improved accuracy: (i) measuring the sample current and applying equation (1), and (ii) measuring the collector current and applying equation (2). To increase secondary electron collection, the current was measured on the first grid of the 120° solid angle collection assembly instead of the final hemispherical screen. Moreover, the use of the 4-grid LEED/AES optics allows measurement of not only total SEE yield, but also the energy distribution function of secondary electrons and

*in-situ* monitoring of the chemical composition and surface structure of the material sample under consideration. In this respect, measurements of the energy distribution of secondary electrons emitted from graphite are provided for a larger range of incident electron energies. The contributions of the three types of secondary electrons to the total yield were calculated and the fraction of backscattered electrons to the total number of secondary electrons was found to match a curve by Scholtz *et al* [15].

## 2. Experimental setup

The experiments were conducted in the Surface Science and Technology Laboratory (SSTL) at the Princeton Plasma Physics Laboratory. A PHI model 15–120 LEED/AES optics consists of an electron gun capable of producing a monoenergetic electron beam with an energy between 3 and 1600 eV, four hemispherical semitransparent grids (the first with 120° solid angle), and a final hemispherical phosphor-coated solid screen. The optics was connected to a PHI model 11–120 LEED electronics control unit. An unconditioned sample of Highly Ordered Pyrolytic Graphite (HOPG) was placed at a working distance of 20 mm in front of the edge of the LEED/AES optics, as shown in figure 1. The collection angle of the LEED/AES optics could not be increased to 180° (e.g. by moving the sample closer to the LEED/AES optics) for the particular sample holder used in these measurements since the sample was placed on a rotational stage and any increase in distance from the rotation axis would make future angular dependence measurements impossible. Additional details on the LEED/AES system and sample mount are available in [23].

The pressure in the vacuum chamber near the sample was measured by an ionization gauge not far from the sample to be  $5 \times 10^{-8}$  Torr. To determine that this background pressure of residual gases in the chamber had no effect on the SEE measurements we considered: (i) scattering of primary and secondary electrons by the residual gases in front of the sample, and (ii) inelastic scattering of primary and secondary electrons within the sample material. The mean free path for scattering of both primary and true secondary electrons (i.e. greater than 50 eV and  $\sim 2$  eV, respectively) by the residual gases at this pressure is calculated to be many orders of magnitude larger than the sample-gun and sample-collector separation ( $\lambda/L \sim 10^5$ , see appendix A), thus this has no effect on our results. In addition, while the chamber pressure is much higher than for typical surface science experiments, this also has no effect on our SEE results on graphite since this is such a chemically inert surface and no adsorbate layers can form at these pressures. Impurities or contamination from surface reactions during exposure of the graphite to atmospheric pressure during mounting of the sample could indeed cause errors (since the inelastic mean free path is only about two monolayers at 50 eV) [24], and future studies will improve control of this situation. However, we note the good agreement between the yield measurements presented here and those measured by previous authors, as will be shown in section 3.

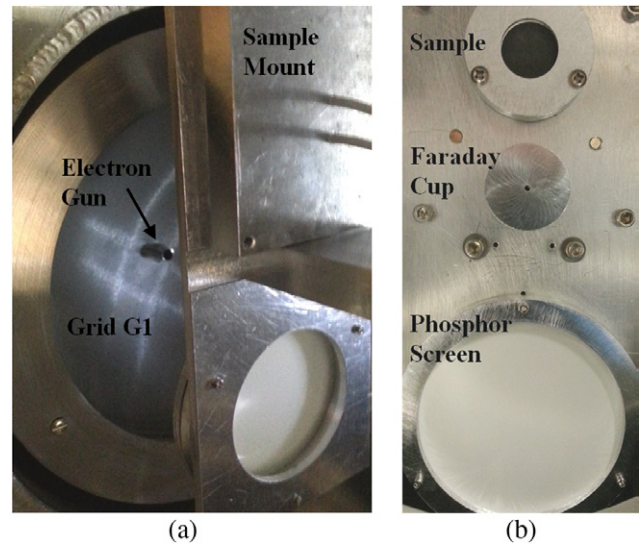


**Figure 1.** Facility for measuring secondary electron emission, including (a) LEED/AES electron optics and (b) sample mount.

The LEED/AES system was used for SEE measurements of electron beams between 50 and 500 eV impacting graphite at normal incidence. The incident current on the sample was measured by applying an increasingly positive voltage on the sample to keep secondary electrons on the sample, while the grids of the LEED/AES optics were kept at ground potential, as shown in figure 2(a). The total SEE current was measured using the LEED/AES optics by applying a positive voltage on the first grid G1, which has a 120° solid angle, to improve collection efficiency while grounding the other grids (see figure 2(b)). Note that measuring the current on all grids of the LEED/AES optics and biasing the first grid G1 minimizes error in the total SEE current due to the emission of tertiary electrons from the grids of the LEED/AES optics.

The secondary electron energy distribution was measured at each primary electron energy by applying a negative retarding potential on grids G2 and G3 of the LEED/AES optics and measuring the current on the final hemispherical screen from electrons with sufficient energy to overcome the applied retarding electric field (see figure 2(c)). The LEED/AES optics thus served as a high pass filter and the electron energy distribution (i.e. number of electrons emitted at a given energy) was calculated by taking the derivative of the measured curve. The electron energy distributions were corrected for difference in contact potential (i.e. difference in work function between the graphite sample and stainless steel retarding grids) to obtain the electron energy with respect to the sample vacuum level (i.e.  $E_{SE} = V_{G2,3} - (\Phi_S - \Phi_{G2,3})$  where  $\Phi_S = 4.6$  eV [25] and  $\Phi_{G2,3} = 4.4$  eV, see figure 3).

Note that for energy distribution measurements, the final hemispherical screen of the LEED/AES optics was biased positive to minimize the emission of tertiary electron from this screen. Tertiary electrons from grids G1 and G2 are negligible since they are of low energy such that they are prevented from reaching the final hemispherical collector by the retarding potentials of grids G2 and G3. Considering the geometry of the

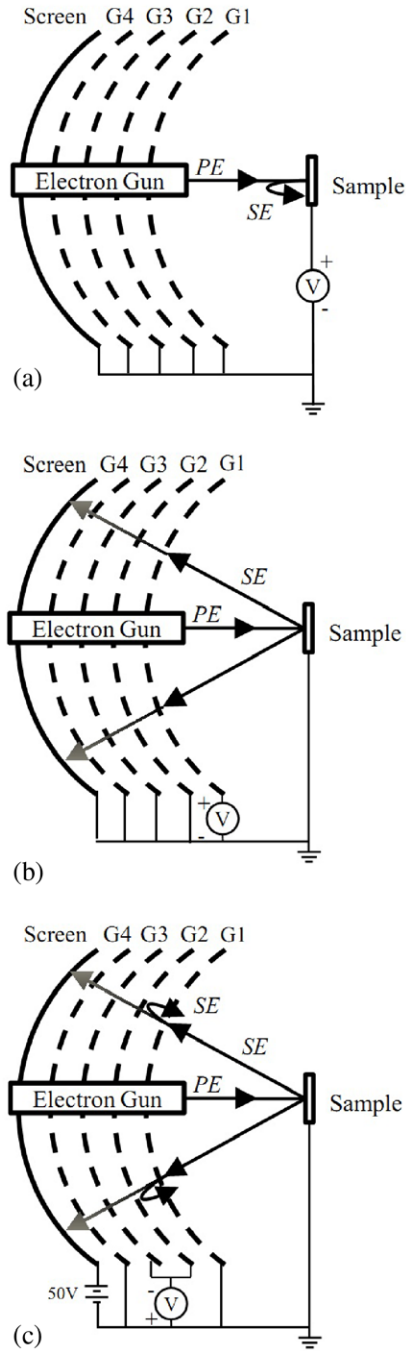


**Figure 2.** Configurations of the 4-grid LEED/AES optics for measuring: (a) primary electron current, (b) secondary electron current, and (c) secondary electron energy distribution function.

LEED/AES optics, about 7.6% and 5.8% of secondary electrons emitted from the sample are calculated to impact grids G3 and G4, respectively, when the LEED/AES optics components are grounded (see Appendix B). Assuming a maximum possible yield of unity for low energy electrons impacting the stainless steel grids, assuming 12% of the tertiary electrons from G3 are measured on the final hemispherical collector (see Appendix B), and assuming all tertiary electrons from G4 are measured on the collector, a maximum of about 7% error (i.e.  $7.6\% \times 12\% + 5.8\% \times 100\%$ ) is calculated for these effects on our energy distribution measurements.

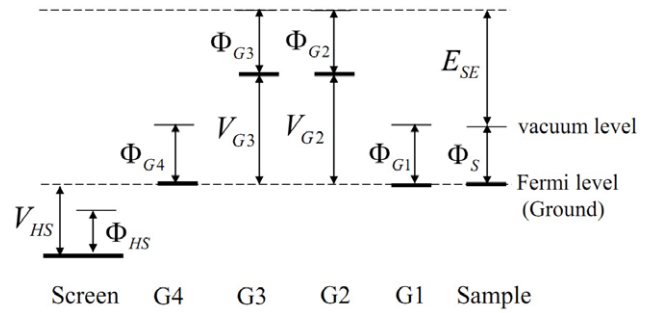


**Figure 3.** Energy level diagram for LEED/AES optics.

### 3. Results and analysis

#### 3.1. Total secondary electron yield

The current from the sample to ground at each of several primary electron beam energies  $E_{PE}$  and sample voltages  $V_S$  are plotted in figure 4. For all curves, the sample electron current increases to an asymptote as  $V_S$  increases. This is due to the increasing number of low energy true secondary electrons that are redirected back to the sample by the applied electric field. Note that while the positive sample voltage increases the primary electron impact energy at the sample, and hence changes the number of secondary electrons emitted, all true secondary electrons are recollected on the sample. Additionally the increased impact energy changes the number and/or energy of backscattered and rediffused electrons, but their contribution is negligible and decreases with primary electron energy. Hence the current on the sample at 50V is primarily from incident primary electrons. As illustrated by figure 4, the SEE current  $I_{SEE}$  can also be measured from the sample current:  $I_S = I_{PE} - I_{SEE}$  where  $I_S$  is the sample current with no bias and  $I_{PE}$  is the sample current at 50V.

Figure 5 shows the current measured on the collector assembly of the LEED/AES optics for each primary electron beam energy  $E_{PE}$  and for various G1 grid (figure 2) voltages  $V_{G1}$ . The electron current to the LEED/AES optics initially increases substantially with increasing G1 voltage as more secondary electrons with emission angles greater than  $60^\circ$  from the surface normal are redirected to the LEED/AES optics by the applied electric field, and then asymptotes. The SEE current for primary electron energies above 100 eV was set to be equal to the current measured when G1 is at 50V (see the dashed line for  $E_{PE} = 500$  eV in figure 5). Note that measuring the SEE current on the entire collector assembly instead of the final collector (as is usually done [13]) negated the need to consider the effective transparency of the grids (which may be different than the optical transparency), thereby improving the accuracy of the measurements. For example, of the SEE current collected on the LEED/AES assembly in figure 5, 85–87% was collected on G1, 12.5–13.5% on G2 and G3, and less than 1.5% on the hemispherical screen when G1 was biased to 50V. This differs from the suggested 17% optical opacity of each of the grids. Also note that by biasing G1, an applied electric field is created in front of the sample that may have possible effects on the

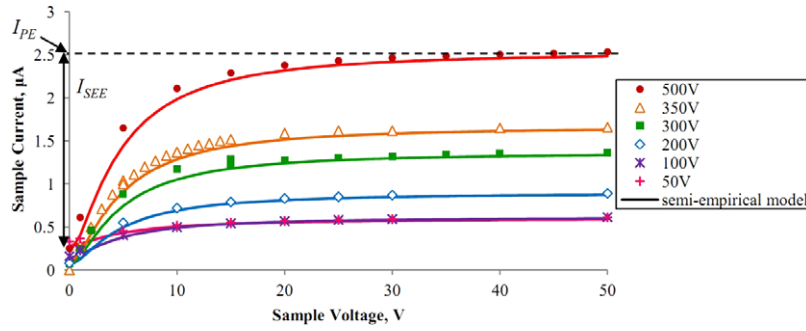


**Figure 4.** Current measured (symbols) from sample to ground for different primary electron energies and sample voltages. For each primary energy, the primary electron current is the sample current when the sample is at 50V (dashed line). The secondary electron current is the difference between the primary electron current and the sample current at zero sample voltage. Calculated currents (solid lines) are also plotted (see section 4).

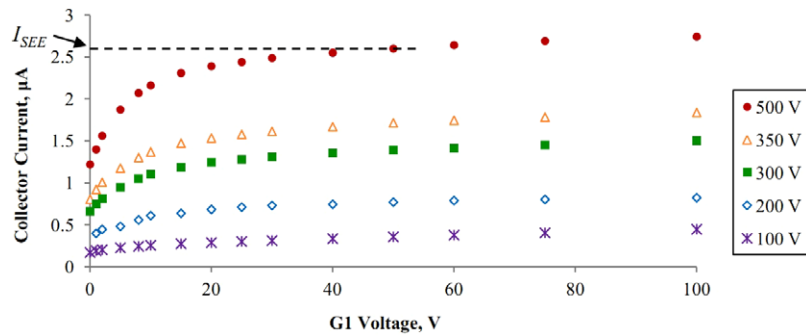


**Figure 5.** Collector current at different primary electron energies and G1 voltages. For each energy, the secondary electron current is found by taking the collector current when G1 is at 50V (dashed line).

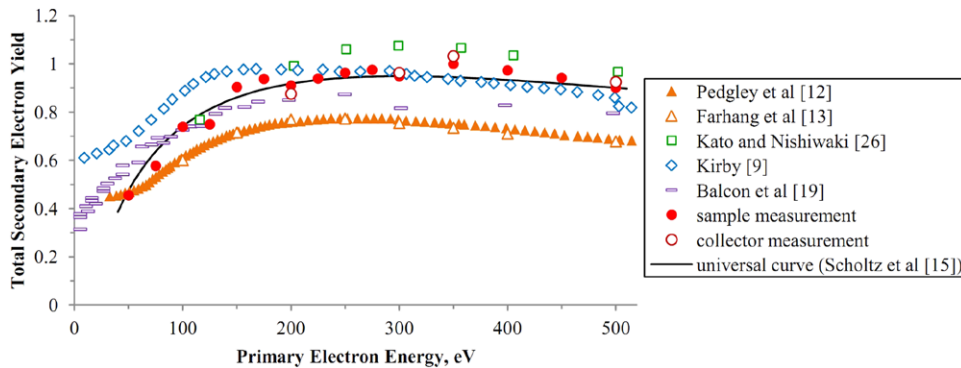


**Figure 6.** Total secondary electron yield for graphite from secondary electron current measurements using the sample current and LEED/AES collector assembly current. Comparisons are made to a universal curve [15] and previous measurements for graphite [9, 12, 13, 19, 26].

measurements (e.g. G1 attracting beam electrons and/or reducing the electron energy at the sample). However, as is seen below, the effects caused by biasing G1 to 50V do not seem to be significant since the SEE current calculated with the collector method compares well to the SEE current from the sample method.

The total SEE yield was calculated using both equations (1) and (2), where the SEE current was measured from the sample current and the LEED/AES optics, respectively, as shown in figure 6. These measurements are compared to an empirical equation for the energy dependence of the total yield found by fitting a Gaussian function of  $\ln(E_{PE}/E_{PE}^{max})$  with variance  $\alpha = 1.6$  to the experimental data:[15]

$$\sigma(E_{PE}) = \sigma_{max} \exp \left\{ - \frac{\left[ \ln \left( \frac{E_{PE}}{E_{PE}^{max}} \right) \right]^2}{2\alpha^2} \right\}, \quad (3)$$

where  $\sigma_{max}$  and  $E_{PE}^{max}$  are the peak total SEE yield and the primary electron energy at which the peak yield occurs, respectively, both of which are material specific. From figure 6, the total yields measured compare well with the empirical equation. Note that for semiconductors, values for  $\sigma_{max}$  and  $E_{PE}^{max}$  are similar to values for conductors since the energy bands near the Fermi level are thermally populated with electrons.

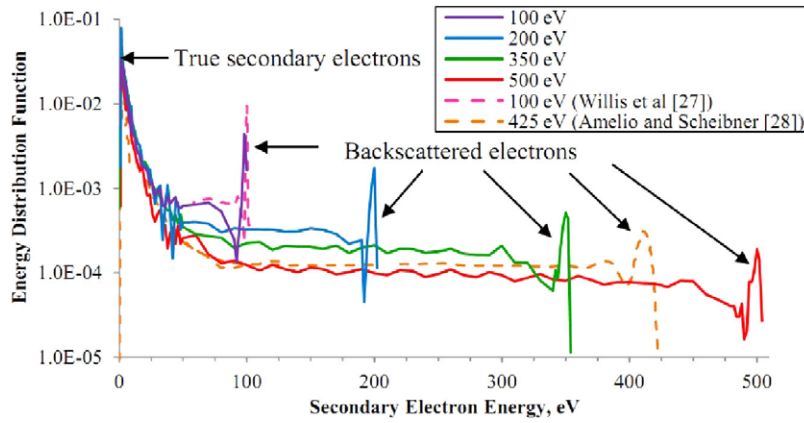


**Figure 7.** Secondary electron energy distributions (with respect to the sample vacuum level) for 100–500 eV primary electrons impacting graphite.

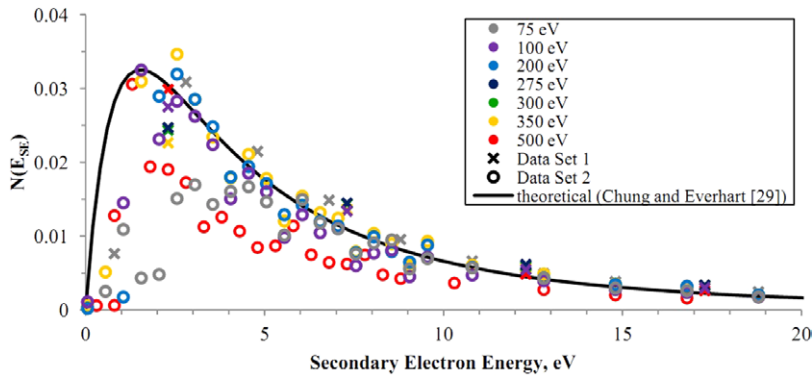


**Figure 8.** Secondary electron energy distributions (with respect to the sample vacuum level) for 75 eV through 500 eV electrons impacting graphite. A theoretical distribution is also given [29].

However, for insulators the maximum yield is larger since the mean free path for secondary electrons en route to the surface is much larger in insulators than the mean free path in metals (due to a lack of free electrons and hence a reduction in electron–electron interactions) [5, 6].

In figure 6 we also plotted the total yield measurements by Pedgley *et al* [12], Farhang *et al* [13], Kato and Nishiwaki [26], Kirby [9], and Balcon *et al* [19]. We postulate that the large variation in experimental measurements is due to the dependence of the yield on the condition of the graphite surface when measurements were taken (e.g. if the sample was processed to remove oxidation and the level of vacuum in the testing chamber). Farhang *et al* [13] and Pedgley *et al* [12] operated in vacuum chambers at  $10^{-9}$  Torr and heated the samples by electron bombardment. The data from Kato and Nishiwaki [26] are for ‘as-received’ graphite samples, as are the present measurements. In figure 6, the present measurements lie close to the measurements from Kato and Nishiwaki.

### 3.2. Secondary electron energy distribution

The measured secondary electron energy distributions for 100, 200, 350, and 500 eV electrons incident on graphite are shown in figure 7, along with previously measured secondary electron energy distributions for 100 eV [27] and 425 eV [28] electrons incident on graphite. There are two main peaks of

$E_{SE}$  in figure 7. The first peak at lower energies (i.e. below 50 eV) is due to true secondary electrons, while the second peak at higher energy (i.e.  $E_{SE} = E_{PE}$ ) is due to backscattered electrons. The latter peak confirms the energy of the primary electron beam. Additional smaller peaks within a few eV of  $E_{PE}$  are due to specific inelastic losses suffered by the backscattered electrons.

Figure 8 shows the secondary electron distribution curves normalized by the primary electron current  $I_{PE}$  for each primary energy:

$$N(E_{SE}) = -\frac{1}{I_{PE}} \frac{I_{HS}(V_{G2,3}^2) - I_{HS}(V_{G2,3}^1)}{V_{G2,3}^2 - V_{G2,3}^1}, \quad (4)$$

where  $E_{SE}$  is the energy of the secondary electrons with respect to the sample vacuum level and  $I_{HS}(V_{G2,3}^i)$  is the current measured on the hemispherical screen of the LEED/AES optics when retarding voltage  $V_{G2,3}^i$  is applied on grids G2 and G3. Focusing on the peak of true secondary electrons ( $E_{SE} < 50$  eV), the distributions are compared to a theoretical result that treats SEE as a three-step process: (i) ionization/excitation of secondary electrons by primary electrons, (ii) transport of secondary electrons to the material surface, and (iii) escape of secondary electrons from the material work function [29]. The energy distribution derived by Chung and Everhart [29] for conducting and non-conducting material,

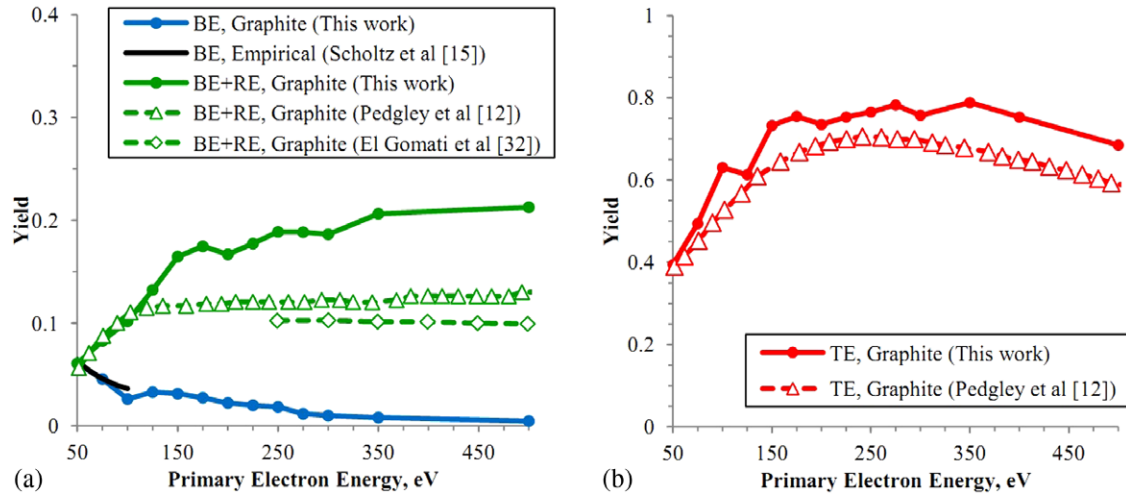


**Figure 9.** Yields of backscattered (BE), rediffused (RE), and true secondary (TE) electrons versus primary electron energy for graphite.

assuming charge accumulation has negligible effect on the beam (e.g. sufficiently short beam exposure times for non-conducting material) [8, 30], is given by

$$N(E_{SE}) = C \frac{E_{SE}}{(E_{SE} + \Phi_S)^4}. \quad (5)$$

where  $C$  is a material constant,  $\Phi_S$  is the work function of the material, and  $E_{SE}$  is the energy of the secondary electron with respect to the sample vacuum level (i.e.  $E_{SE} = V_{G2,3} - (\Phi_S - \Phi_{G2,3})$ , see figure 3). From figure 8, at higher secondary electron energies (i.e. above 10 eV) the measured energy distributions agree well with the theoretical distribution for the range of primary electron energies examined. Below 10 eV, there is a large scatter in the measured distributions due to the low resolution of  $V_{G2,3}$  applied. However, the distributions are seen to follow the trend of the theoretical curve with a maximum between 1.3 and 3 eV.

Figure 8 also suggests that the secondary electron energy distribution is a non-accelerated distribution (i.e. the distribution starts from zero energy as opposed to a positive energy). This is particularly important for electric propulsion devices (i.e. Hall-effect thrusters). While an accelerated distribution always leads to a two-stream instability within the device, a non-accelerated energy distribution may or may not lead to an instability, depending on the number of secondary electrons emitted [31].

The contributions to the electron yield from backscattered, rediffused, and true secondary electrons can be separated from the energy distributions in figure 7. In figure 9 we plot the yields of backscattered electrons, the sum of backscattered and rediffused electrons, and true secondary electrons for graphite between 50 and 500 eV, along with an empirical curve for the backscattered yield:[15]

$$\eta(E_{PE}) = \sigma \exp[1.59 + 3.75 \ln E_{PE} - 1.37 (\ln E_{PE})^2 + 0.12 (\ln E_{PE})^3] \quad (6)$$

where  $\eta$  is the yield of backscattered electrons and  $E_{PE}$  is between 5 and 100 eV. In deriving equation (6), Scholtz *et al* [15] fit a single curve to data from various materials. From

figure 9 the experimentally measured yield for graphite follows a similar curve. The yield of backscattered electrons increases as the primary electron energy decreases. This agrees with theory that as the primary electron energy is reduced, backscattered electrons become increasingly important. However, the exact behavior at very low primary electron energy (below approximately 30 eV) is still uncertain since previous measurements at low primary energies were difficult due to the limitation of electron guns to produce beams of ample primary electrons at low energies (where the current is space charge limited) and/or due to the presence of stray electric and magnetic fields (including the Earth's magnetic field) that can affect low energy electron beams. For example, Balcon *et al* [19] warned that the absence of a magnetic shield in their measurements (where the distance from the electron gun to the sample was larger than the electron gyroradius) could have possibly prevented beam electrons below 10 eV from reaching the sample surface.

Also plotted in figure 9 are curves for the true secondary yield and the backscattered and rediffused yield measured by Pedgley *et al* [12] and El Gomati *et al* [32] for graphite. Our results for the backscattered and rediffused yield follow the trend of these two prior reports, i.e. the yield increases with primary electron energy at low energies (below 125 eV) and is relatively insensitive to energy at higher primary energies. Our measured backscattered and rediffused yields are consistent with Pedgley *et al* [12] at low primary electron energies, but are larger than values measured by Pedgley *et al* [12] and El Gomati *et al* [32] at higher energies. The true secondary yield determined herein also follows the trend of Pedgley *et al* [12] with values comparable with their measured values. As mentioned previously in section 3.1, quantitative differences with the results of Pedgley *et al* [12] could be due to differences in samples, their preparations, as well as differences in measurement systems.

#### 4. Semi-empirical model

To further validate the sample method for determining primary electron current and SEE current, universal empirical



and theoretical equations were used to reproduce the curves in figure 4. Assuming the change in sample current  $I_S$  with sample bias voltage  $V_S$  is due to true secondary electrons that are recollected and to increased primary electron impact energies,

$$I_S(V_S) = I_{PE} - I_{BE} - I_{TE} \\ = I_{PE} \{1 - \eta(E_{PE} + V_S) - \delta(E_{PE} + V_S)[1 - f(V_S)]\} \quad (7)$$

where  $I_{PE}$ ,  $I_{BE}$ , and  $I_{TE}$  are the currents from primary, back-scattered, and true secondary electrons, respectively. The yield for true secondary electrons is

$$\delta(E_{PE}) = \sigma(E_{PE}) - \eta(E_{PE}), \quad (8)$$

where  $\sigma$  and  $\eta$  are given by equation (3) and equation (6), respectively. The fraction  $f$  of true secondary electrons with energy below  $E_{SE} = V_S$  (i.e. recollected by the sample) is calculated from equation (5),

$$f(V_S) = \frac{N(E_{SE} \leq V_S)}{N_{tot}}. \quad (9)$$

The calculated curves are plotted with the measured curves in figure 4. The fair agreement over the full range of sample bias voltages for the range of primary electron energies examined serves to validate the experimental setup and approach, as well as the equations for total SEE yield and energy distribution.

## 5. Conclusions

A facility utilizing 4-grid LEED/AES optics was developed to provide comprehensive characterization of SEE properties of conducting materials, including the total SEE yield and secondary electron energy distribution of emitted electrons. Measurements of total electron yield were made for primary electrons between 50 and 500 eV using a conventional 4-grid LEED/AES optics, which can also be utilized for *in-situ* monitoring of material chemical composition and crystal structure. Measurements were made for graphite, which is the material used for plasma-facing components in many applications such as plasma thrusters, and divertors and limiters of magnetic fusion devices.

In order to achieve accurate SEE measurements, two methods were used: (i) measuring the current on a positively biased sample, and (ii) measuring the current on the LEED/AES optics with a positively biased first grid G1. Use of the sample method to measure primary electron current (a technique used by this and previous authors [15]) was validated with development of a semi-empirical model. The accuracy of the collector method was improved by measuring the SEE current on the entire collection assembly instead of the final collector (as is usually done), negating the need to consider the transparency of the grids. Hence, results for the total yield calculated with the two methods of SEE measurements agreed well and were within the spread of yield measurements found in the literature for graphite and with values calculated using an empirical equation valid for conducting materials. The energy distribution of emitted secondary electrons from graphite (useful for modeling plasma-wall interactions in fusion and

plasma devices) was measured. The fraction of backscattered, rediffused, and true secondary electrons calculated from the energy distribution function agreed well with empirical results.

The facility and LEED/AES optics used can be easily upgraded to measure the angular dependence of the SEE properties and extended to measure SEE properties of non-conducting materials by pulsed operation as done in [33].

## Acknowledgments

The authors would like to thank Dr Angela Capece of the Surface Science and Technology Laboratory at PPPL for much technical and scientific support, and Chenggang Jin for assistance in data collection. The authors are also grateful to Dr Igor Kaganovich of PPPL and Dr Taylor Matlock of UCLA for fruitful discussions of secondary electron emission physics and effects in plasma. Funding for this research was provided by the Air Force Office of Scientific Research under AFOSR Grants FA9550-11-1-0282 and FA9550-09-1-0695, the US Department of Energy under Contract No DE-AC02-09CH11466, and the UCLA School of Engineering and Applied Science. BEK acknowledges support of this work by the Air Force Office of Scientific Research under AFOSR Grant FA9550-14-1-0053.

## Appendix A

The mean free path  $\lambda$  for electrons in  $N_2$  gas (as an example) is given by

$$\lambda = \frac{1}{\sigma_{e-N_2} n} \quad (A.1)$$

where  $\sigma_{e-N_2}$  is the electron-nitrogen collision cross-section and  $n$  is the density of nitrogen. For 2 eV true secondary electrons leaving the sample,  $\sigma_{e-N_2}$  is  $3 \times 10^{-19} \text{ m}^2$  [34] and the mean free path at  $5 \times 10^{-8} \text{ Torr}$  is  $2 \times 10^3 \text{ m}$ , which is five orders of magnitude larger than the distance between the sample and LEED/AES optics. A similar calculation can be done to show there is no effect due to scattering of primary electrons by the residual gases in front of the sample: for the lowest primary electron energy of 50 eV,  $\sigma_{e-N_2}$  is  $8 \times 10^{-20} \text{ m}^2$  [34] and the mean free path at  $5 \times 10^{-8} \text{ Torr}$  is  $7 \times 10^3 \text{ m}$ , which is larger. We also note that at the electron energies and currents considered here, there is no thermal or electron-induced desorption.

## Appendix B

Considering the geometry of the experiment, where the LEED/AES optics are approximately 20 mm from the sample and the grids of the LEED/AES optics are 2.7 mm apart, the half-angle  $\theta$  from the sample center to the edge of each grid, as shown in figure B1, is calculated to have the value given in table B1. Assuming no obstruction between the sample and the respective grid, assuming zero grid transparency, and assuming a cosine distribution for emitted electrons, the fraction  $g$  of secondary electrons collected on each grid is

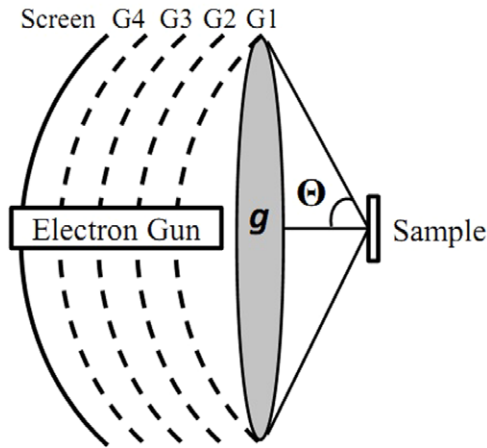


Figure B1. Schematic of grid half-angle.

Table B1. Secondary Electron Collection on the LEED/AES Optics.

	G1	G2	G3	G4	Screen
$\theta$	60°	56.6°	53.5°	50.8°	48°
$g$	0.75	0.70	0.65	0.60	0.55
$I/I_{SEE}$	12.8%	9.8%	7.6%	5.8%	26.2%

$$g = \int_0^{2\pi} \int_0^{\theta} \cos\theta \sin\theta d\theta d\varphi = 1 - \cos^2\theta. \quad (B.1)$$

However, there are a number of grids of which each has the same transparency  $t$  (i.e. 83% not zero) and a number of grids  $N$  in front of the grid under consideration. Hence, the fraction of secondary electrons from the sample that are collected on each grid of the LEED/AES optics when each grid is grounded is calculated to be

$$\frac{I}{I_{SEE}} = gt^{N-1}(1 - t). \quad (B.2)$$

When calculating the number of tertiary electrons from G3 that are measured on the final hemispherical collector plate, it is assumed that  $(1 - t)$  of tertiary electrons hit G2,  $t$  of those pass through G3, and  $t$  of those pass through G4). Hence 12% of the tertiary electrons from G3 are measured on the final hemispherical collector.

References

[1] Hobbs G D and Wesson J A 1967 Heat flow through a Langmuir sheath in the presence of electron emission *Plasma Phys.* **9** 85–7  
 [2] Sydorenko D, Smolyakov A, Kaganovich I and Raites Y 2006 Kinetic simulation of secondary electron emission effects in Hall thrusters *Phys. Plasmas* **13** 014501  
 [3] Graves T P, Spektor R, Stout P and Axley A 2009 Transient-mode multipactor discharge *Phys. Plasmas* **16** 083502  
 [4] Cimino R, Collins I R, Furman M A, Pivi M, Ruggiero F, Rumolo G and Zimmermann F 2004 Can low-energy

electrons affect high-energy physics accelerators? *Phys. Rev. Lett.* **93** 014801  
 [5] Bruining H 1954 *Physics and Applications of Secondary Electron Emission* (London: Pergamon)  
 [6] Dekker A J 1958 *Secondary Electron Emission (Solid State Physics - Advances in Research and Applications)* vol 6 ed F Seitz and D Turnbull (New York and London: Academic) pp 251–311  
 [7] Wells O C 1974 *Scanning Electron Microscopy* (New York: McGraw-Hill)  
 [8] Seiler H 1983 Secondary electron emission in the scanning electron microscope *J. Appl. Phys.* **54** R1–18  
 [9] Kirby R E 2004 Instrumental effects in secondary electron yield and energy distribution measurements *Proc. 31st ICFA Advanced Beam Dynamics Workshop on Electron-Cloud Effects: E-CLOUD'04 (Napa, CA, USA, 19–23 April 2004)* (CERN) ed M Furman et al (Geneva, Switzerland) CERN-2005-001 pp 107–11  
 [10] Lye R G and Dekker A J 1957 Theory of secondary emission *Phys. Rev.* **107** 977–81  
 [11] Vaughan J R M 1989 A new formula for secondary emission yield *IEEE Trans. Electron Devices* **36** 1963–7  
 [12] Pedgley J M, McCracken G M, Farhang H and Blott B H 1992 Measurements of secondary electron emission for fusion related materials *J. Nucl. Mater.* **196–198** 1053–8  
 [13] Farhang H, Napchan E and Blott B H 1993 Electron backscattering and secondary electron emission from carbon targets: comparison of experimental results with Monte Carlo simulations *J. Phys. D: Appl. Phys.* **26** 2266–71  
 [14] Thomas E W 1995 Particle-impact induced electron ejection from surfaces *Int. Nuclear Data Committee Report (Vienna, Austria, February 1995)* (IAEA Nuclear Data Section) INDC (NDS)-322 pp 1–35  
 [15] Scholtz J J, Dijkkamp D and Schmitz R W A 1996 Secondary electron emission properties *Philips J. Res.* **50** 375–89  
 [16] Ordonez C A and Peterkin R E Jr 1996 Secondary electron emission at anode, cathode, and floating plasma-facing surfaces *J. Appl. Phys.* **79** 2270–4  
 [17] Zamoski N D, Kumar P, Watts C, Svimonishvili T, Schamiloglu E and Gaudet J A 2006 Secondary electron yield measurements from material with application to collectors of high-power microwave devices *IEEE Trans. Plasma Sci.* **34** 642–51  
 [18] Belhaj M, Roupie J, Jbara O, Puech J, Balcon N and Payan D 2012 Electron emission at very low electron impact energy: experimental and Monte-Carlo results *Proc. Joint INFN-CERN-EuCARD-AccNet Workshop on Electron-Cloud Effects: E-CLOUD'12 (La Biodola Isola d'Elba, Italy, 5–9 June 2012)* (CERN) (Geneva, Switzerland) CERN-2013-002 pp 137–9  
 [19] Balcon N, Payan D, Belhaj M, Tondou T and Inguibert V 2012 Secondary electron emission on space materials: evaluation of the total secondary electron yield from surface potential measurements *IEEE Trans. Plasma Sci.* **40** 282–90  
 [20] Woods M E, Hopkins B J and McCracken G M 1985 Secondary electron yield measurements from limiter materials in the Joint European Torus *Surf. Sci.* **162** 928–33  
 [21] Woods M E, Hopkins B J, Matthews G F, McCracken G M, Sewell P M and Farhang H 1987 An investigation of the secondary-electron emission of carbon samples exposed to a hydrogen plasma *J. Phys. D: Appl. Phys.* **20** 1136–42  
 [22] Cimino R and Collins I R 2004 Vacuum chamber surface electronic properties influencing electron cloud phenomena *Appl. Surf. Sci.* **235** 231–5  
 [23] Patino M I, Raites Y, Koel B E and Wirz R E 2013 Application of Auger spectroscopy for measurement of secondary electron emission from conducting material for electric propulsion devices *Proc. 33rd Int. Electric Propulsion Conf. (Washington, DC, USA, 6–10 October 2013)* pp 1–8

- [24] Seah M P and Dench W A 1979 Quantitative electron spectroscopy of surfaces: a standard data base for electron inelastic mean free path in solids *Surf. Interface Anal.* **1** 2–11
- [25] Takahashi T, Tokailin H, and Sagawa T 1985 Angle-resolved ultraviolet photoelectron spectroscopy of the unoccupied band structure of graphite *Phys. Rev. B* **32** 8317–24
- [26] Kato S and Nishiwaki M 2003 Secondary electron emission from metals and graphites *Accelerator Tech. Design Report for J-PARC* (11 March 2003) ed Y Yamazaki *et al* (Japan Atomic Energy Research Institute and High Energy Accelerator Research Organization) pp 2.3.8–7
- [27] Willis R F, Fitton B, and Painter G S 1974 Secondary-electron emission spectroscopy and the observation of high-energy excited states in graphite: theory and experiment *Phys. Rev. B* **9** 1926–37
- [28] Amelio G F and Scheibner E J 1968 Auger spectroscopy of graphite single crystals with low energy electrons *Surf. Sci.* **11** 242–54
- [29] Chung M S and Everhart T E 1974 Simple calculation of energy distribution of low energy secondary electrons emitted from metals under electron bombardment *J. Appl. Phys.* **45** 707–9
- [30] Hoffmann R C 2010 *Electron-Induced Electron Yields of Uncharged Insulating Materials M.S. Thesis*, Utah State University, Logan, Utah
- [31] Sydorenko D, Smolyakov A, Kaganovich I, and Raitses Y 2007 Effects of non-Maxwellian electron velocity distribution function on two-stream instability in low-pressure discharges *Phys. Plasmas* **14** 013508
- [32] El Gomati M M *et al* 2008 Theory experiment comparison of electron backscattering factor from solids at low electron energy (250–5,000 eV) *Scanning* **30** 2–15
- [33] Dunaveasky A, Raitses Y and Fisch N J 2003 Secondary electron emission from dielectric materials of a Hall thruster with segmented electrodes *Phys. Plasmas* **10** 2574–7
- [34] Okhrimovskyy A, Bogaerts A and Gijbels R 2002 Electron anisotropic scattering in gases: a formula for Monte Carlo simulations *Phys. Rev. E* **65** 037402